

Event-guided Deblurring of Unknown Exposure Time Videos

Taewoo Kim, Jungmin Lee, Lin Wang and Kuk-Jin Yoon
Visual Intelligence Lab., KAIST, Korea

{intelpro, jeanmichel, wanglin, kjyoon}@kaist.ac.kr

Abstract

Video deblurring is a highly ill-posed problem due to the loss of motion information in the blur degradation process. Since event cameras can capture apparent motion with a high temporal resolution, several attempts have explored the potential of events for guiding video deblurring. These methods generally assume that the exposure time is the same as the reciprocal of the video frame rate. However, this is not true in real situations, and the exposure time might be unknown and dynamically varies depending on the video shooting environment (e.g., illumination condition). In this paper, we address the event-guided video deblurring assuming dynamically variable unknown exposure time of the frame-based camera. To this end, we first derive a new formulation for event-guided video deblurring by considering the exposure and readout time in the video frame acquisition process. We then propose a novel end-to-end learning framework for event-guided video deblurring. In particular, we design a novel Exposure Time-based Event Selection (ETES) module to selectively use event features by estimating the cross-modal correlation between the features from blurred frames and the events. Moreover, we propose a feature fusion module to effectively fuse the selected features from events and blur frames. We conduct extensive experiments on various datasets and demonstrate that our method achieves state-of-the-art performance. Our project code and pretrained models will be available.

1. Introduction

Motion blur often occurs due to the non-negligible exposure time of the frame-based cameras. Any motion during the video recording makes the sensor observe an averaged signal from different points in the scene [23, 45]. Video deblurring is a task aiming at restoring sharp video frames from the motion-blurred ones. This task is a highly ill-posed problem due to the loss of motion information in the blur degradation process, especially in the complex real-world scene [1, 6, 9]. Recently, deep learning (DL)-based approaches have achieved great success in modeling general motion blur and recovering sharp frames from the motion-blurred frames [20, 32, 50, 56]. However, they are limited to

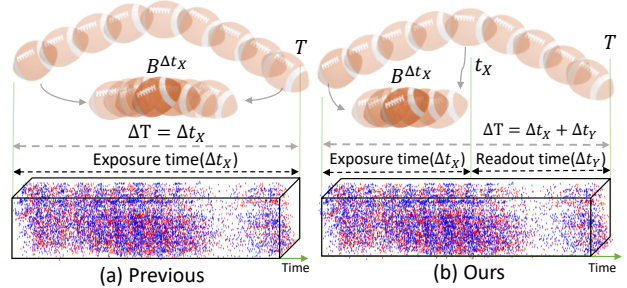


Figure 1. The motivation of our work. The figure shows the image formation setting assumed in (a) previous event-guided methods and (b) our work. Here, ΔT represents the shutter period. From above to bottom, continuous latent images, video frame acquisition, corresponding event streams ($E^{\Delta T}$), respectively. Previous methods generally assume that the exposure time is the same as the reciprocal of the video frame rate, while ours considers the actual exposure time for selectively using events.

specific scenarios and may fail to recover the sharp frames for the severe motion blur.

Event cameras are bio-inspired sensors that encode the per-pixel intensity change asynchronously with high temporal resolution. Many endeavors have been engaged in reconstructing image/video from event streams [19, 30, 39–42, 60]. However, the reconstructed results from the events only may lose texture details. Consequently, several attempts have leveraged events for guiding video deblurring [9, 17, 26, 39, 54], trying to take advantage of frame-based and event cameras. As shown in Fig. 1(a), these methods generally assume that the exposure time is the same as the reciprocal of the video frame rate and perform the video deblurring guided by the events within the exposure time. However, this assumption may not be valid in real situations since the video frame acquisition process generally consists of two phases: exposure phase (X) and readout phase (Y) [5, 56], as illustrated in Fig. 1(b). In the exposure phase, the shutter of the camera opens and receives lights. In the readout phase, the camera clears charge from the serial register, and the pixel value is digitalized. The total time, the reciprocal of the frame rate, is called the shutter period, not exposure time. Since the motion blur of the frame-based camera occurs only in the exposure phase rather than the

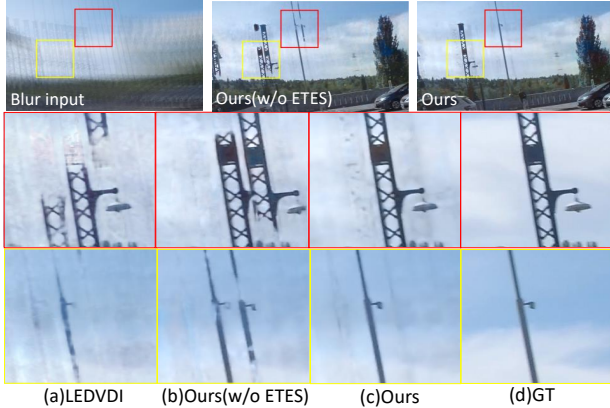


Figure 2. Results of video deblurring on the unknown exposure time videos. Our proposed ETES module enables to restore a sharp frame more reliably than existing event-guided deblurring methods, e.g., LEDVDI [17], which was trained on the same dataset.

readout phase, it is crucial to use the events during the exposure phase within the shutter period. However, the exposure time is not always known, and furthermore, it can dynamically vary depending on the imaging environments when the auto-exposure function turns on. For that reason, we assume the exposure time is unknown when performing the event-guided video deblurring, as shown in Fig. 1(b), to consider more practical situations. This assumption can lead to significant performance changes. If we apply the existing event-guided video deblurring methods, e.g., [17], for an unknown exposure time video frame, the performance degrades, as shown in Fig. 2(a).¹ Therefore, it is necessary to infer the actual exposure time to use events rightly for video deblurring.

To this end, we derive a new formulation of event-guided deblurring for the unknown exposure time videos. Accordingly, we propose an end-to-end learning framework. As the exposure time is assumed to be unknown, we first propose an event selection module called the Exposure Time-based Event Selection (ETES). The proposed module extracts the relevant events within the shutter period by estimating the temporal correlation between events and blur frames features. As such, only the event features corresponding to the exposure time are automatically selected for guidance. Second, we propose a new module for events-frame feature fusion, inspired by the attention mechanism [38]. Such a fusion module leads to more robust feature representation learning. Lastly, we make two synthetic and one real-world event datasets by simulating dynamically variable unknown exposure time of a frame-based camera. In summary, our contributions are three-fold. (I) We study and formulate an event-guided video deblurring for unknown exposure time videos. (II) Based on the formulation, we design a novel

¹This result is obtained by using all the events during the shutter period without knowing the actual exposure time.

ETES module to select event features and propose a feature fusion module to use complementary information of events and frames. (III) We conduct experiments on two synthetic and real-world datasets and demonstrate that our method achieves state-of-the-art performance for deblurring.

2. Related works

Image and Video Deblurring. DL has been broadly applied to image and video deblurring. Earlier works, e.g., [33], utilized convolutional neural networks (CNNs) with frame alignment and merged multiple frames based on the homography for video deblurring. The baseline networks have been improved by applying more sophisticated network structures or learning methods, e.g., recurrent neural networks (RNN) [7, 21, 27, 35, 45, 57], multi-scale architecture [2, 4, 20], adversarial training [14, 15, 51–53], multi-stage approaches [3, 49, 50], video frame alignment [11, 16, 24, 43, 58] in an end-to-end learning manner.

Event-guided Video Deblurring. The event cameras show higher temporal resolution and HDR properties. To leverage the advantages of event cameras, recent works focus on event-guided video deblurring. Pan *et al.* [25, 26] first proposed a video deblurring framework by formulating an event-based double integral model (EDI). Although they show the effectiveness of the formulation, they often fail to reconstruct the scene details due to the noisy contrast threshold of the events. To solve the aforementioned issues, Jiang *et al.* [9] introduced a DL-based video deblurring framework by using an RNN-based network architecture and a directional event filtering module. More recently, Lin *et al.* [17] proposed a CNN-based framework driven by an event-based physical model for video deblurring. Shang *et al.* [31] proposed an event-guided video deblurring framework to exploit the non-consecutively blurry video frames. Concurrently, Xu *et al.* [48] proposed a self-supervised learning framework that utilizes real events to alleviate performance degradation due to the domain gap between real and synthetic data. These works generally assume the exposure time is the same as the shutter period. However, as aforementioned, this assumption is not valid in many real situations. *Unlike these works, we propose a novel framework for unknown exposure time videos.* Accordingly, we first propose an ETES module to extract the valuable event features corresponding to the unknown exposure time. We then propose a frame-event feature fusion method to leverage the complementary information.

3. Method

3.1. Formulation

We first derive a new formulation by considering the video frame acquisition process to perform event-guided video deblurring for unknown exposure time videos.

Event Selection A video frame acquisition consists of the

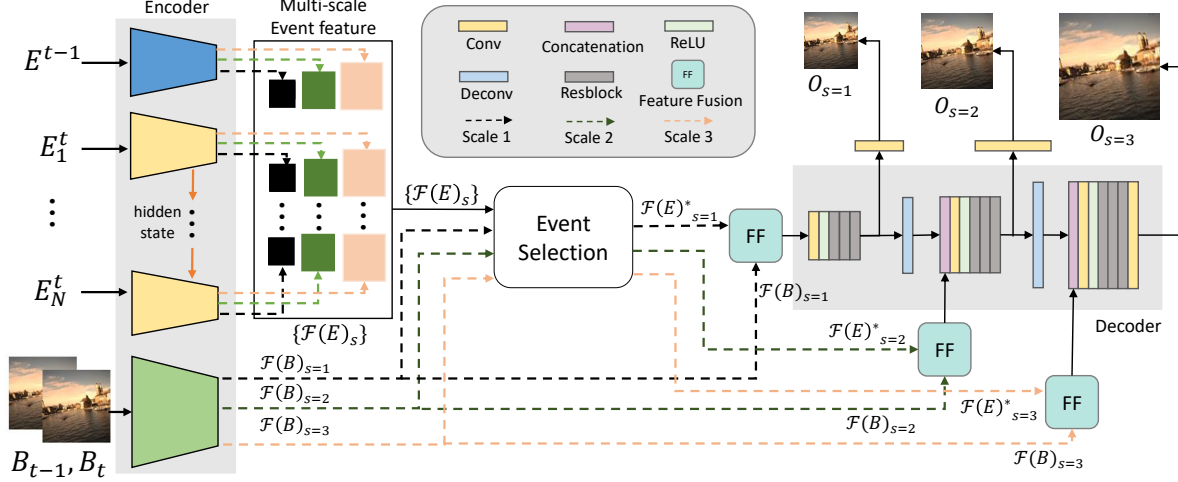


Figure 3. Overview of the proposed framework. For the encoder, blue, yellow, and green boxes represent an event encoder for the past part, an shared RNN-based event encoder for the current part, and a blur-frame encoder, respectively.

exposure phase X and readout phase Y , as depicted in Fig. 1. We denote the duration of the exposure phase as Δt_X and the readout phase as Δt_Y . The summation of two phases (shutter period), ΔT , represents the time to acquire one video frame. By the nature of frame-based cameras, motion blur only occurs during the exposure phase X . In contrast, events are generated in the exposure phase X and the readout phase Y . Therefore, it is imperative to use events during the exact duration of the exposure phase Δt_X only. The existing event-guided video deblurring methods [17, 26] assume that the exposure time is equal to the shutter period; $\Delta T = \Delta t_X$. By contrast, our goal is to estimate the temporal correlation between the motion-blurred frame and the event during ΔT to handle the unknown exposure time Δt_X . A motion-blurred frame can be expressed as the temporal average of N latent frames during the exposure time as

$$B(x, y) \simeq \frac{1}{N} \sum_{i=1}^N L_{\tau_i}(x, y), \quad (1)$$

where $B(x, y)$ denotes a blur frame and $L_{\tau_i}(x, y)$ is the i -th latent frame at τ_i . For event cameras, an event $e_t(x, y, t, p)$ is triggered when the log intensity change exceeds a contrast threshold β . Here, t denotes the timestamp, and $p \in \{-1, +1\}$ is the polarity indicating the sign of intensity changes. The output event tensor E^t can be represented as:

$$E^t = \Phi \left\{ \log \left(\frac{I^t(x, y)}{I^{t-1}(x, y)} \right), \beta \right\}, \quad (2)$$

where $I^t(x, y)$ is the intensity value at triggering time stamp t , and $\Phi\{\lambda, \beta\}$ denotes the condition of event generation: when $\lambda \geq \beta$, positive events are generated, and vice versa.

Given two consecutive frames, $I^{t_1}(x, y)$ and $I^{t_2}(x, y)$, the events are triggered by intensity changes between them.

Accordingly, we can derive the relationship between two intensity images based on event generation, formulated as:

$$I^{t_2}(x, y) \simeq I^{t_1}(x, y) \sum_{t_1}^{t_2} (\beta e_t) = I^{t_1}(x, y) \tilde{R}(x, y), \quad (3)$$

By combining Eq.(1) and Eq.(3), we can represent a motion-blurred frame as follows:

$$B(x, y) \simeq I^t \left(\frac{1}{N} \sum_{i=1}^N \tilde{R}_i(x, y) \right) = I^t(x, y) S(x, y) \quad (4)$$

where $I^t(x, y)$ denotes a middle latent frame, which is the result of deblurring, and $S(x, y)$ is the summation of residual matrix $\tilde{R}_i(x, y)$. According to Eq.(4), we need to estimate a residual matrix $S(x, y)$ corresponding to the exposure time. However, since the exact exposure time is unknown, we aim at estimating the temporal correlation between the blurred frames and events during ΔT . That is, to estimate $S(x, y)$, we find a function f_{θ^*} that approximates a set of events $\{E^{\Delta t_X}\}$ based on $\{E^{\Delta T}\}$ and the blur frame $B^{\Delta t_X}$ as

$$f_{\theta^*} \sim \{E^t \mid \psi(E^t, B^{\Delta t_X}) > 0\}; \quad t \in \{0, T\} \quad (5)$$

where $\psi(E^t, B^{\Delta t_X})$ is a conditional function obtained by calculating the temporal correlation between E^t and $B^{\Delta t_X}$. With respect to E^t , a function $\psi(E^t, B^{\Delta t_X})$ is true when the intensity change corresponding to E^t exists in the motion-blurred frame $B^{\Delta t_X}$ and, vice versa. As such, only the events within the exposure time are selected as guidance.

Event-guided Video Deblurring Through the above formulation, we can select event streams $\{E^{\Delta t_X}\}$ among

$\{E^{\Delta T}\}$ for the unknown exposure time Δt_X . Accordingly, we aim at recovering an intermediate sharp video frame from the motion-blurred ones $B^{\Delta t_X}$ using $\{E^{\Delta t_X}\}$.

3.2. The Proposed Framework

Based on the formulation, we propose a novel end-to-end learning framework. To feed event streams to DNNs, we need to embed them to the fixed size tensor-like format. The voxel grid [59] is a well-designed event representation as it preserves the spatio-temporal information of events.

$$E(x_i, y_i, t) = \sum_{(x_i, y_i)} p_i \max(0, 1 - |t - t_i^*|) \quad (6)$$

Here, $t_i^* = (B-1)(t_i)/t_N$ is the normalized time stamp. B is temporal bins for discretizing the time dimension. We use 16 temporal bins of the voxel grid for all the experiments.

3.2.1 Overview

An overview of the proposed framework is depicted in Fig. 3, which utilizes a pyramid structure in a coarse-to-fine manner. It consists of *two* major components: *event selection and feature fusion*. For event selection (Sec.3.2.2), we first encode the embedded events via an RNN-based encoding network. Then, we propose a novel ETES module to select the beneficial event features *without any supervision*. Finally, in Sec. 3.2.3, we propose a new feature fusion module that efficiently exploits the complementary information of events and frames.

3.2.2 Event Selection

Recurrent Encoding for Embedded Events. To extract features from events, recent works widely adopt 2D CNNs [17, 59]; however, they are less effective in preserving temporal information for the event selection under unknown exposure time (Eq.5). For this reason, we devise a new RNN cell-based encoding method of the event feature to preserve temporal information inspired by recent frame-based video deblurring works [21, 57]. Specifically, we first divide the events into the past shutter period part $\{E^{t-1}\}$ and the current shutter period part $\{E^t\}$. For the past part $\{E^{t-1}\}$, we extract a feature pyramid $\{\mathcal{F}(E^{t-1})_s\}$ using a 2D CNN block with the scale index $s \in \{1, 2, 3\}$. For the current part $\{E^t\}$, we design RNN-based encoders with shared weights to extract features for preserving temporal information, as shown in Fig. 3. Considering the temporal information of the current part, we first divide the voxel grid into N temporal units with an equal time interval Δt_{unit} . Thus, we get temporally divided event units $E_n^t \in \mathbb{R}^{2 \times H \times W}$ with the temporal index $n \in \{1, \dots, N\}$. We then recursively update the hidden state of the RNN cell to reinforce temporal coherence between consecutive event units. As such, we generate N hierarchical feature maps at each scale index s for the current part

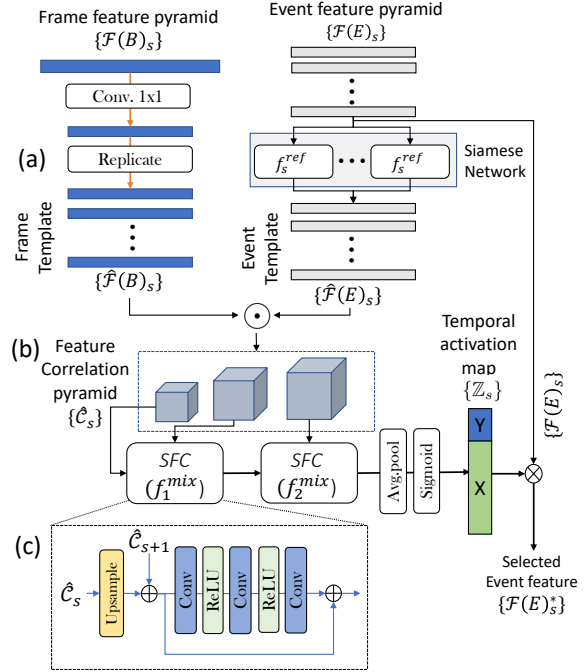


Figure 4. The network structure of the proposed Event Selection Module. ‘‘SFC’’ denotes the scale-fusion CNN block. See text for more details.

$\{\mathcal{F}(E_1^t)_s, \dots, \mathcal{F}(E_N^t)_s\}$. The extracted features of the current and past parts are concatenated to form a feature pyramid, denoted by $\{\mathcal{F}(E)_s\} \in \mathbb{R}^{(N+1) \times C_s^U \times H_s \times W_s}$, where C_s^U, H_s, W_s denotes the numbers of unit channels, height, and width at scale index s , respectively. For brevity, we denote $N + 1$ as T .

Exposure Time-based Event Selection (ETES) Module.

Through encoding, we obtain the event and frame feature pyramids $\{\mathcal{F}(E)_s\}$ and $\{\mathcal{F}(B)_s\}$, respectively. To approximate Eq.(5), we now aim to select the beneficial event features corresponding to the dynamically varying unknown exposure time of the frame-based camera. However, there exist two crucial challenges. The first one is how to preprocess event features (with complete temporal information) and frame features (with missing temporal information). The second is how to better discover the cross-modal relationship between events and frames by aggregating the feature pyramid obtained from two different modalities. To this end, we propose a novel ETES module *without any supervision*, as depicted in Fig. 4. The main idea is to temporally mine the essential channels of event features based on the multi-scale cross-modal correlation. In detail, we aim to suppress the event feature corresponding to the duration of the readout phase by calculating the similarity between the blur frame feature and the event feature along with the temporal flow. As depicted in Fig. 4(a), we first pre-process the event and frame features to calculate cross-modal cor-

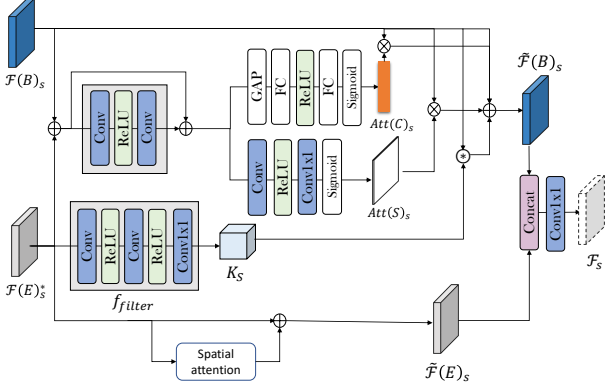


Figure 5. Proposed feature fusion module. In the figure, \otimes denotes dynamic convolution operation with a generated convolution filter.

relation at multiple visual scales. For the frame features at scale s , we first compress them by applying the point-wise convolution to reduce spatial information loss. Then, we replicate the compressed frame features to have the same temporal dimension as the event features. The operations are formulated as:

$$\hat{\mathcal{F}}(B)_s = \xi(\text{Conv}_{1 \times 1, s}(\mathcal{F}(B)_s)), \quad (7)$$

where $\text{Conv}_{1 \times 1, s}$ is the point-wise convolution at scale s such that $\mathbb{R}^{C_s^U \times H_s \times W_s} \rightarrow \mathbb{R}^{C_{s=1}^U \times H_s \times W_s}$. Here, ξ denotes the replication operation along the temporal dimension to form frame template features $\hat{\mathcal{F}}(B)_s$ such that $\mathbb{R}^{C_{s=1}^U \times H_s \times W_s} \rightarrow \mathbb{R}^{T \times C_{s=1}^U \times H_s \times W_s}$. This allows calculating the cross-modal correlation in unit time interval Δt_{unit} .

For the event features at scale s , we leverage a siamese network [13] to modulate them to effectively maintain the temporal information within Δt_{unit} , as shown in Fig. 4(a). We apply this w.r.t. each temporal unit of the event features, $f_s^{\text{ref}}: \mathbb{R}^{C_s^U \times H_s \times W_s} \rightarrow \mathbb{R}^{C_{s=1}^U \times H_s \times W_s}$. The features are concatenated along the temporal dimension to form event template features $\hat{\mathcal{F}}(E)_s$. We finally apply the group normalization [47] to these two template features to mitigate the extreme modality differences. Through pre-processing both the event and frame features, we can get two feature templates at each scale s . As shown in Fig. 4(b), it is imperative to explore the correlations from the feature pyramids to select the most beneficial events. For this reason, we aggregate these two feature templates via the Hadamard product \odot for all scales as

$$\hat{\mathcal{C}}_s = \text{ReLU}(\hat{\mathcal{F}}(E)_s \odot \hat{\mathcal{F}}(B)_s) \quad (8)$$

where the feature correlation $\hat{\mathcal{C}}_s \in \mathbb{R}^{T \times C_{s=1}^U \times H_s \times W_s}$ with ReLU for removing noisy correlation. Finally, we get a rich collection of feature correlation $\{\mathcal{C}_s\}$ seen from multiple visual aspects. As illustrated in Fig. 4(c), we merge the collection of correlation features by designing a scale-fusion

convolutional (SFC) block. In particular, SFC aims to form a multi-scale temporal activation map $\{\mathcal{Z}_s\} \in \mathbb{R}^{T \times C_s^U \times 1 \times 1}$ in three steps. SFC upsamples the correlation features at scale s , followed by an element-wise addition with the features at scale $s+1$. It then propagates the most beneficial correlation information in a top-down manner. In such a way, it effectively enables the merge of lower-level to a higher-level cross-modal correlation between the frame and event. Lastly, we squeeze the output tensor on the spatial dimension by average-pooling followed by a sigmoid activation function. The output tensor is the condensed temporal activation map $\mathcal{Z}_{s=1} \in \mathbb{R}^{T \times C_{s=1}^U \times 1 \times 1}$. We then interpolate $\mathcal{Z}_{s=1}$ to get the temporal activation map at each scale s $\mathcal{Z}_s \in \mathbb{R}^{T \times C_s^U \times 1 \times 1}$ as

$$\mathcal{F}(E)_s^* = \mathcal{Z}_s \otimes \mathcal{F}(E)_s \quad (9)$$

where \otimes denotes channel-wise multiplication. As such, the ETES module filters and selects the event features w.r.t. unknown exposure time of the frame, as shown in Fig. 8. Each of the selected event feature pyramids $\{\mathcal{F}(E)_s^*\}$ is fed into the feature fusion module of each scale, as depicted in Fig. 3.

3.2.3 Feature Fusion Module

The event features $\mathcal{F}(E)_s^*$ are selected via event selection module. We notice that the blur frame features $\mathcal{F}(B)_s$ contain rich semantic and texture information, while the selected event features contain clear edge and motion cues. Therefore, it is meaningful to leverage the information from event features to complement the frame features. It is possible to use existing feature fusion methods directly, e.g., RGB-D [34, 55]. However, as events are remarkably different from the frame, naively using these methods rather degrades the video deblurring performance. Consequently, we propose a novel event-frame feature fusion module for video deblurring, as depicted in Fig. 5. Our idea is to leverage the event features to mine the discriminative channels and spatial information from the blur frame features. That is, we first calibrate the frame and event features via element-wise summation. As a result, the frame features of blurry regions are highlighted through calibration due to the motion cues of the event features. We then employ the global average pooling(GAP) to obtain global statistics, which are fed into a fully connected(FC) layer to obtain a channel attention vector for the frame features $\text{Att}(C)_s \in \mathbb{R}^{T \times C_s \times 1 \times 1}$. Meanwhile, we extract spatial attention maps $\text{Att}(S)_s$ to attain the spatial statistics from calibrated features. As such, only the important blur frame features related to video deblurring are highlighted, and the unnecessary information are suppressed. Moreover, we design a filter generation block f_{filter} (see Fig. 5) to generate a position-specific convolution filter $K_s = f_{\text{filter}}(\mathcal{F}(E)_s^*)$ from the selected event features $\mathcal{F}(E)_s^*$, inspired by kernel

prediction networks [8, 17, 18, 22]. The filtered features are formulated as:

$$\begin{aligned} \tilde{\mathcal{F}}(B)_s &= \mathcal{F}(B)_s + \text{Att}(C)_s \otimes \mathcal{F}(B)_s \\ &+ \text{Att}(S)_s \cdot \mathcal{F}(B)_s + K_s \otimes \mathcal{F}(B)_s \end{aligned} \quad (10)$$

where \otimes denotes convolution operation and \otimes denotes channel-wise multiplication. For event features, we only apply spatial attention [46] from the selected event feature $\mathcal{F}(E)_s^*$. The fused features \mathcal{F}_s at each scale is obtained by concatenating the enhanced event features $\tilde{\mathcal{F}}(E)_s$ and the filtered frame features $\tilde{\mathcal{F}}(B)_s$, followed by a 1×1 convolution. The procedure can be represented as follows:

$$\mathcal{F}_s = \text{Conv}_{1 \times 1}(\text{Concat}(\tilde{\mathcal{F}}(E)_s, \tilde{\mathcal{F}}(B)_s)). \quad (11)$$

Lastly, the fused feature $\{\mathcal{F}_s\}$ are separately fed into the decoder to reconstruct a sharp video, as shown in Fig. 3. The outputs of the decoder consist of sharp video frames at each scale, represented as $\{O_s\}$. We use the charbonnier loss [10] for optimization, and the total loss is:

$$\mathcal{L}_{total} = \sum_{s=0}^2 \lambda_s \sqrt{\|O_{gt,s} - O_s\|^2 + \varepsilon^2} \quad (12)$$

We empirically set to $\varepsilon = 10^{-3}$ for all experiments.

4. Experiments

4.1. Datasets and Implementation Details

Synthetic datasets We train and test the proposed framework on the GoPro dataset [20], widely used for video deblurring. We then directly test with the test split of the Adobe datasets [33] using the trained model on the GoPro dataset. For both datasets, we follow an official data split, and events are generated from the high frame rate video using an event simulator (ESIM) [29]. We synthesize blurry video by averaging the video frames. To mimic the real video frame acquisition, we follow the method in [56]. We discard several video frames to simulate the readout time. We denote the number of video frames of the exposure phase as m and that of the readout phase as n . We downsample the original video from 240fps to 15fps with $m + n = 16$. We set the frame number m of the exposure phase as an odd number $m = \{9, 11, 13, 15\}$ larger than 8 to clearly examine the deblurring effect. As such, we get a synthetic dataset that simulates various exposure times with 15fps. We denoted this dataset as “dataset-m-n”.

Real-world datasets To evaluate our method on real-world events, we use the High-Speed Event-RGB dataset (HS-ERGB) dataset [37]. The HS-ERGB dataset provides high frame rate video (~ 140 fps) and spatially aligned events streams using a dual-camera setup consisting of an RGB camera and event camera. Similar to video frame generation on the synthetic dataset, we attain the blurry video

by averaging the high-speed video frames with the setting $m+n = 10$. We set the frame number of the exposure phase as an odd number $m = \{5, 7, 9\}$. We split the training and test sequence based on the scene change and motion speed.

Implementation Details Our frameworks are implemented using PyTorch [28]. We train our framework for 170 and 200 epochs on the synthetic and real-world datasets, respectively. For all datasets, we utilize the batch size of 8 and ADAM [12] optimizer to update weight using a multi-step scheduler with an initial learning rate $1e^{-4}$ and decay rate $\gamma = 0.5$. For data augmentation, we apply random cropping(256×256) to the event and frame for the same position. We adopt the dynamic convolution operation from the implementation of STFAN [58]. λ_s of Eq.(12) are set to $\{1, 0.1, 0.1\}$ for each scale. For quantitative evaluation, we use common evaluation metrics PSNR and SSIM [44].

4.2. Experimental Results

We compare with Nah *et al.* [20] and DMPHN [50] feeding into the RGB frame with embedded event data to their networks(denoted as Nah *et al.* \dagger , DMPHN \dagger). In addition, we reimplement the state-of-the-art (SOTA) event-guided video deblurring methods [17](denoted as LEDVDI \dagger) based on the code provided by the authors. We keep the original network architecture with modification of our event representation [59].

Synthetic datasets For a fair comparison, we *retrain* the one frame-based method [57] and three event-guided methods(LEDVDI \dagger and Nah *et al.* \dagger and DMPHN \dagger) on our training dataset. We also compare with the SOTA frame-based methods using official pre-trained models [3, 4, 15, 20, 36, 49, 50, 52] provided by the authors. As clearly shown in Tab. 1, our method surpasses the frame-based and event-guided methods by a large margin on the two datasets. Compared to the frame-based method, the average PSNR score of our method improves from 4.98dB to 9.41dB in the GoPro-15fps, from 6.83dB to 9.07dB in the Adobe-15fps. As we maximize the number of video frames corresponding to the exposure phase, the performance gap between our method and frame-based competitors widens from 7.14dB to 10.49dB in the GoPro-15-1. This indicates our method achieves better results on challenging motion blur frames. Compared to the event-guided method, our method still shows better results by from 1.72 dB to 2.04dB in the GoPro-15fps, by from 1.92 to 2.43dB in the Adobe-15fps in terms of the average PSNR. As shown in Fig. 6, our methods can restore sharper texture details than the previous event-guided methods under extreme blur conditions. In particular, only our methods can restore the sophisticated tree structure and thin street lamp.

Real-world datasets contain clearly different scenes from the synthetic dataset, so we *retrain* the SOTA frame-based methods [4, 17, 20, 57] and event-guided methods

Table 1. Quantitative evaluation on a synthetic dataset. Asterisk(*) means retraining our training dataset. † denotes the event-guided method. The **Bold** and underline denote the best and the second-best performance, respectively. We trained our method on the GoPro dataset and directly applied it to the Adobe dataset. The same notation and typography are applied to the following tables.

Method	GoPro -15fps								Adobe-15fps							
	GoPro-9-7		GoPro-11-5		GoPro-13-3		GoPro-15-1		Adobe-9-7		Adobe-11-5		Adobe-13-3		Adobe-15-1	
	PSNR	SSIM														
Nah <i>et al.</i> [20]	28.89	0.930	27.76	0.914	26.70	0.895	25.74	0.876	28.29	0.914	27.35	0.900	26.59	0.888	25.96	0.878
DMPHN [50]	31.21	0.946	30.39	0.936	28.75	0.914	26.83	0.880	29.17	0.920	28.22	0.905	27.21	0.888	26.31	0.872
Kupyn <i>et al.</i> [15]	30.18	0.932	29.10	0.918	28.11	0.903	27.21	0.888	29.81	0.924	28.85	0.913	28.09	0.903	27.51	0.894
DBGAN [52]	32.15	0.955	31.44	0.945	29.25	0.921	26.99	0.881	29.91	0.927	28.82	0.912	27.70	0.895	26.69	0.878
BANet [36]	33.02	0.961	32.38	0.956	30.89	0.941	28.93	0.915	31.01	0.943	29.96	0.929	28.84	0.913	27.90	0.898
MPRNet [49]	33.77	0.967	32.65	0.959	31.24	0.946	29.66	0.927	31.20	0.945	30.17	0.933	29.05	0.919	28.16	0.906
MIMO-UNet [4]	33.34	0.964	32.39	0.956	30.74	0.940	28.52	0.908	30.83	0.939	29.76	0.925	28.57	0.908	27.51	0.892
HINet [3]	33.60	0.965	32.86	0.960	31.26	0.945	29.09	0.917	31.06	0.944	30.08	0.932	28.90	0.915	27.91	0.901
ESTRNN* [57]	29.97	0.929	28.93	0.916	27.96	0.901	27.04	0.885	28.36	0.907	27.45	0.893	26.72	0.881	26.10	0.870
Nah <i>et al.</i> †* [20]	35.33	0.971	35.09	0.969	34.92	0.968	34.54	0.965	34.66	0.968	34.17	0.965	<u>34.28</u>	<u>0.966</u>	33.68	<u>0.962</u>
DMPHN† [50]	34.61	0.964	34.46	0.965	34.09	0.963	33.71	0.960	34.25	0.966	33.84	0.964	<u>33.52</u>	<u>0.962</u>	33.13	0.959
LEDVDI† [17]	35.13	0.969	34.86	0.967	34.47	0.964	34.10	0.961	<u>34.70</u>	<u>0.970</u>	<u>34.24</u>	<u>0.967</u>	33.87	0.964	<u>33.70</u>	0.962
Ours†	37.16	0.980	36.82	0.978	36.52	0.976	36.23	0.975	36.63	0.977	36.23	0.975	35.92	0.973	35.68	0.972

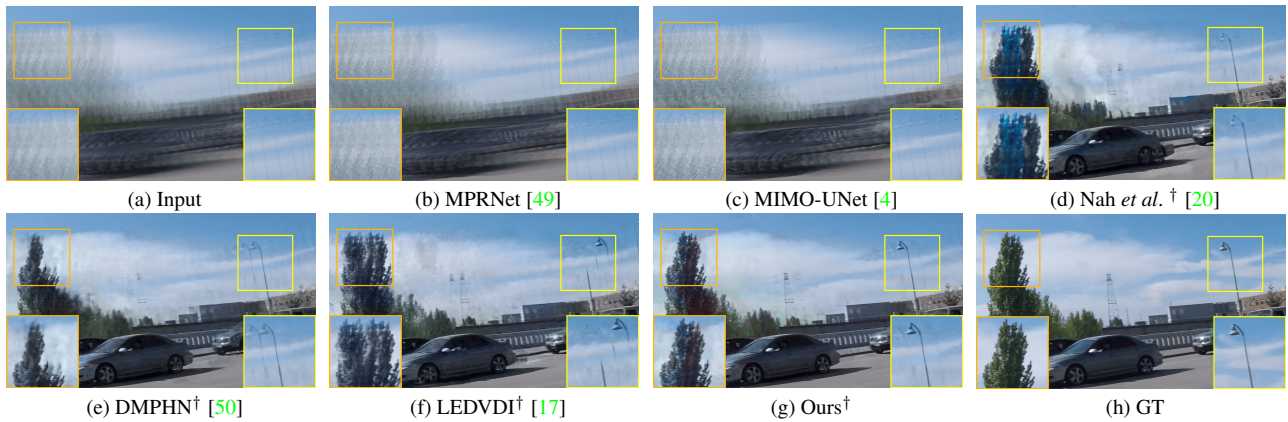


Figure 6. Visual results on the Adobe datasets

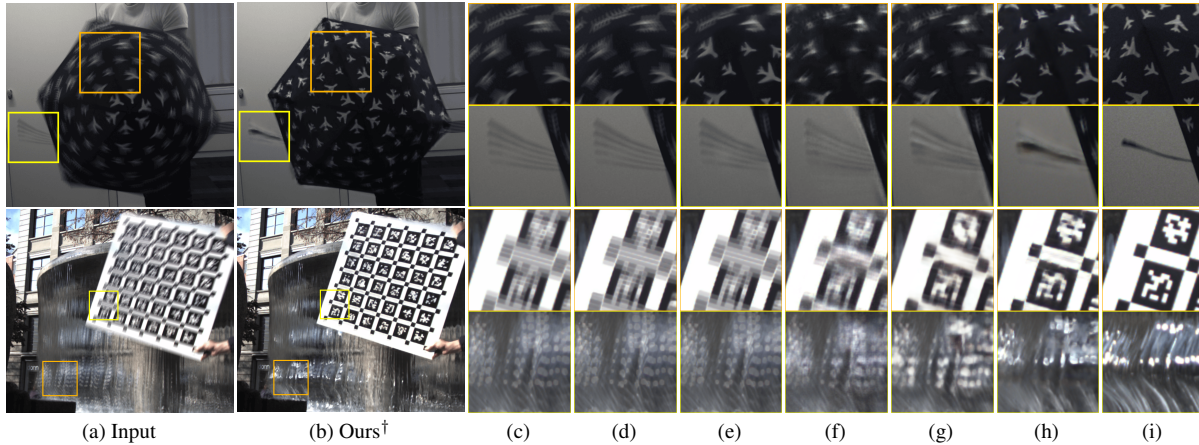


Figure 7. Visual results on the real-world datasets. The two larger images on the left are the blurred inputs and our network outputs, respectively. For better visualization, the magnified cropped images are displayed. From left to right: (c) Input, (d) MPRNet [49], (e) MiMO-UNet [4], (f) DMPHN† [50], (g) LEDVDI† [17], (h) Ours†, (i) GT.

(LEDVDI†, Nah *et al.* †, DMPHN†) to our real-world datasets. In Tab. 2, we report the deblurring performance compared with frame-based and event-guided methods. Our method outperforms all these frame-based and event-guided methods. Compared with the frame-based methods,

the performance gap between our framework and frame-based methods varies from 1.81 to 2.17dB in terms of the average PSNR. Moreover, we still have a performance improvement by 1.39dB to 2.27dB compared with the event-guided methods. Figure 7 shows the visual comparison with

Table 2. Quantitative evaluation on real-world dataset

Method	HS-ERGB					
	5-5		7-3		9-1	
	PSNR	SSIM	PSNR	SSIM	PSNR	SSIM
Nah <i>et al.</i> * [20]	30.51	0.891	29.56	0.876	28.88	0.866
ESTRNN* [57]	30.19	0.888	29.25	0.873	28.58	0.863
MPRNet [49]	29.92	0.888	29.32	0.875	29.92	0.868
MIMO-UNet* [4]	30.98	0.894	29.99	0.879	29.28	0.869
Nah <i>et al.</i> †* [20]	31.39	0.896	30.33	0.883	29.88	0.873
DMPHN†* [50]	30.18	0.879	29.66	0.869	29.02	0.860
LEDVDI†* [17]	30.95	0.895	30.32	0.885	30.25	0.877
Ours†	32.53	0.905	31.88	0.893	31.27	0.883

Table 3. Quantitative evaluation on the dataset of various fps

	GoPro-24fps		GoPro-20fps		GoPro-10fps	
	PSNR	SSIM	PSNR	SSIM	PSNR	SSIM
LEDVDI†	37.33	0.979	36.28	0.975	33.67	0.958
Ours†	38.91	0.985	38.37	0.983	35.86	0.973

Table 4. Ablation study on individual components of the proposed method on the GoPro-15fps dataset

RE	MS	ETES	FF	9-7	11-5	13-3	15-1	Avg.
				PSNR	PSNR	PSNR	PSNR	PSNR
				36.15	35.94	35.5	35.05	35.66
✓				36.38	36.08	35.63	35.33	35.86
✓	✓			36.69	36.18	35.9	35.68	36.11
✓	✓		✓	36.79	36.47	36.13	35.86	36.31
✓	✓	✓		37.07	36.74	36.4	36.1	36.58
✓	✓	✓	✓	37.21	36.87	36.56	36.27	36.73

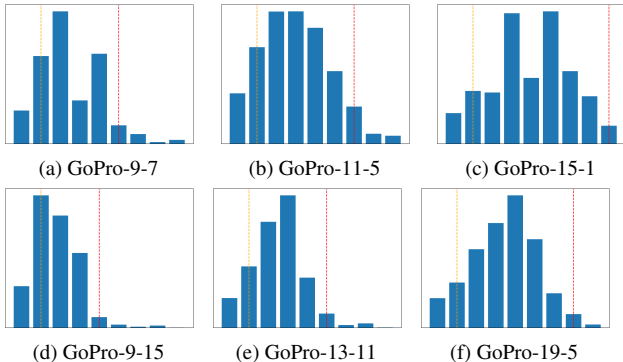


Figure 8. The visualization results of the average temporal activation map of the ETES module for the test split of the GoPro-15fps and GoPro-10fps dataset. The horizontal and vertical axes represent the temporal axis and the average amount of channel activation, respectively. The yellow and red dotted lines indicate the start and end of the exposure time, respectively. Note that almost all activated regions are within the exposure phase.

the previous methods. In the first row (“spinning umbrella” sequence), we confirm that our method effectively restored a sharp image even under extreme non-linear motion, as shown in the patches. In the second row (“fountain Bellevue” sequence), our method restores not only the non-linear motion but also illumination changes well.

Experiments on various FPS We validate the deblurring effectiveness by varying the FPS in the GoPro dataset. Each dataset corresponds to 24, 20, and 10 fps, and 3, 4, and 9 types of time intervals (the exposure time) exist. We train LEDVDI† and our method for each dataset. As shown in

Tab. 3, our method consistently outperforms the previous event-guided methods. Moreover, we confirm that most of the activated regions of the ETES module are within the exposure phase, as illustrated in Fig. 8(d), (e), (f).

4.3. Ablation study

We analyzed the performance contribution of our network modules. All ablation experiments are performed on the GoPro-15fps dataset with models trained for 170 epochs.

Recurrent Encoding (RE) To demonstrate the effectiveness of RE, we compare the model using 2D CNNs and the proposed shared-RNN cell for embedding event streams. From the 1st and 2nd rows of Tab. 4, we observe a performance gain (+0.20db) when using RE. When using the 2D CNNs for encoding events, temporal information lying in the event streams is not well preserved, adversely affecting video deblurring. Furthermore, if we use a multi-scale loss function in the training step (denoted as “MS” in Tab. 4), we observe a performance gain (+0.25db).

ETES module is the most crucial module in our method. To verify the effectiveness, we validate the deblurring performance with and without this module. From the 3rd and 5th rows of Tab. 4, we observe a significant performance improvement (+0.47db) in terms of the average PSNR. As illustrated in Fig. 2(b) and (c), the qualitative result demonstrates that estimating the unknown exposure time helps recover sharp details. For a better understanding of the working principle of the ETES module, we plot the average distribution of the activated event channels for each temporal unit according to various unknown exposure times in Fig. 8(a), (b), (c). Here, we confirm that all activations are within the exposure phase and hardly activate at the read-out phase. This figure demonstrates that the ETES module successfully helps estimate the temporal boundary between exposure and readout phases without any supervision.

Feature Fusion Module For cross-modality fusion of frame and event features, the simplest way is to use a concatenation of two features to fuse two different modality features. In Tab. 4, by comparing 3th and 4th rows, we can observe performance improvement (+0.20db). The proposed feature fusion module can better utilize the complementary information from frame and event features.

5. Concluding Remarks

This paper studied and formulated a new research problem of event-guided deblurring for unknown exposure time videos. We proposed a novel end-to-end framework. In detail, we proposed a method of selectively using event features by estimating the feature correlation of different modalities of events and frames. Moreover, extensive experiments demonstrated our method significantly surpasses existing event-guided and frame-based deblurring methods.

References

- [1] Dawit Mureja Argaw, Junsik Kim, Francois Rameau, and In So Kweon. Motion-blurred video interpolation and extrapolation. In *Proceedings of the AAAI Conference on Artificial Intelligence*, volume 35, pages 901–910, 2021. 1
- [2] Stephan Brehm, Sebastian Scherer, and Rainer Lienhart. High-resolution dual-stage multi-level feature aggregation for single image and video deblurring. In *Proceedings of the IEEE/CVF Conference on Computer Vision and Pattern Recognition (CVPR) Workshops*, June 2020. 2
- [3] Liangyu Chen, Xin Lu, Jie Zhang, Xiaojie Chu, and Chengpeng Chen. Hinet: Half instance normalization network for image restoration. In *Proceedings of the IEEE/CVF Conference on Computer Vision and Pattern Recognition*, pages 182–192, 2021. 2, 6, 7
- [4] Sung-Jin Cho, Seo-Won Ji, Jun-Pyo Hong, Seung-Won Jung, and Sung-Jea Ko. Rethinking coarse-to-fine approach in single image deblurring. *arXiv preprint arXiv:2108.05054*, 2021. 2, 6, 7, 8
- [5] T.J. Fellers and Davidson M.W. Digital camera readout and frame rates. <https://hamamatsu.magnet.fsu.edu/articles/readoutandframerates.html>, 2020-06-04. 1
- [6] Hongyun Gao, Xin Tao, Xiaoyong Shen, and Jiaya Jia. Dynamic scene deblurring with parameter selective sharing and nested skip connections. In *Proceedings of the IEEE/CVF Conference on Computer Vision and Pattern Recognition (CVPR)*, June 2019. 1
- [7] Tae Hyun Kim, Kyoung Mu Lee, Bernhard Scholkopf, and Michael Hirsch. Online video deblurring via dynamic temporal blending network. In *Proceedings of the IEEE International Conference on Computer Vision*, pages 4038–4047, 2017. 2
- [8] Xu Jia, Bert De Brabandere, Tinne Tuytelaars, and Luc V Gool. Dynamic filter networks. *Advances in neural information processing systems*, 29:667–675, 2016. 6
- [9] Zhe Jiang, Yu Zhang, Dongqing Zou, Jimmy Ren, Jiancheng Lv, and Yebin Liu. Learning event-based motion deblurring. In *Proceedings of the IEEE/CVF Conference on Computer Vision and Pattern Recognition*, pages 3320–3329, 2020. 1, 2
- [10] Justin Johnson, Alexandre Alahi, and Li Fei-Fei. Perceptual losses for real-time style transfer and super-resolution. In *European conference on computer vision*, pages 694–711. Springer, 2016. 6
- [11] Tae Hyun Kim, Mehdi SM Sajjadi, Michael Hirsch, and Bernhard Scholkopf. Spatio-temporal transformer network for video restoration. In *Proceedings of the European Conference on Computer Vision (ECCV)*, pages 106–122, 2018. 2
- [12] Diederik P Kingma and Jimmy Ba. Adam: A method for stochastic optimization. *arXiv preprint arXiv:1412.6980*, 2014. 6
- [13] Gregory Koch, Richard Zemel, Ruslan Salakhutdinov, et al. Siamese neural networks for one-shot image recognition. In *ICML deep learning workshop*, volume 2. Lille, 2015. 5
- [14] Orest Kupyn, Volodymyr Budzan, Mykola Mykhailych, Dmytro Mishkin, and Jiří Matas. Deblurgan: Blind motion deblurring using conditional adversarial networks. In *Proceedings of the IEEE Conference on Computer Vision and Pattern Recognition (CVPR)*, June 2018. 2
- [15] Orest Kupyn, Tetiana Martyniuk, Junru Wu, and Zhangyang Wang. Deblurgan-v2: Deblurring (orders-of-magnitude) faster and better. In *The IEEE International Conference on Computer Vision (ICCV)*, Oct 2019. 2, 6, 7
- [16] Dongxu Li, Chenchen Xu, Kaihao Zhang, Xin Yu, Yiran Zhong, Wenqi Ren, Hanna Suominen, and Hongdong Li. Arvo: Learning all-range volumetric correspondence for video deblurring. In *Proceedings of the IEEE/CVF Conference on Computer Vision and Pattern Recognition*, pages 7721–7731, 2021. 2
- [17] Songnan Lin, Jiawei Zhang, Jinshan Pan, Zhe Jiang, Dongqing Zou, Yongtian Wang, Jing Chen, and Jimmy SJ Ren. Learning event-driven video deblurring and interpolation. In *ECCV (8)*, pages 695–710, 2020. 1, 2, 3, 4, 6, 7, 8
- [18] Ben Mildenhall, Jonathan T Barron, Jiawen Chen, Dillon Sharlet, Ren Ng, and Robert Carroll. Burst denoising with kernel prediction networks. In *Proceedings of the IEEE Conference on Computer Vision and Pattern Recognition*, pages 2502–2510, 2018. 6
- [19] Sayed Mohammad Mostafaviifahani, Yeongwoo Nam, Jonghyun Choi, and Kuk-Jin Yoon. E2sri: Learning to super-resolve intensity images from events. *IEEE Transactions on Pattern Analysis & Machine Intelligence*, (01):1–1, 2021. 1
- [20] Seungjun Nah, Tae Hyun Kim, and Kyoung Mu Lee. Deep multi-scale convolutional neural network for dynamic scene deblurring. In *Proceedings of the IEEE conference on computer vision and pattern recognition*, pages 3883–3891, 2017. 1, 2, 6, 7, 8
- [21] Seungjun Nah, Sanghyun Son, and Kyoung Mu Lee. Recurrent neural networks with intra-frame iterations for video deblurring. In *Proceedings of the IEEE/CVF Conference on Computer Vision and Pattern Recognition*, pages 8102–8111, 2019. 2, 4
- [22] Simon Niklaus, Long Mai, and Feng Liu. Video frame interpolation via adaptive convolution. In *Proceedings of the IEEE Conference on Computer Vision and Pattern Recognition*, pages 670–679, 2017. 6
- [23] Mehdi Noroozi, Paramanand Chandramouli, and Paolo Favaro. Motion deblurring in the wild. In *GCPR*, pages 65–77. Springer, 2017. 1
- [24] Jinshan Pan, Haoran Bai, and Jinhui Tang. Cascaded deep video deblurring using temporal sharpness prior. In *Proceedings of the IEEE/CVF Conference on Computer Vision and Pattern Recognition (CVPR)*, June 2020. 2
- [25] Liyuan Pan, Richard Hartley, Cedric Scheerlinck, Miaomiao Liu, Xin Yu, and Yuchao Dai. High frame rate video reconstruction based on an event camera. *IEEE Transactions on Pattern Analysis and Machine Intelligence*, 2020. 2
- [26] Liyuan Pan, Cedric Scheerlinck, Xin Yu, Richard Hartley, Miaomiao Liu, and Yuchao Dai. Bringing a blurry frame alive at high frame-rate with an event camera. In *Proceed-*

- ings of the *IEEE/CVF Conference on Computer Vision and Pattern Recognition*, pages 6820–6829, 2019. 1, 2, 3
- [27] Dongwon Park, Dong Un Kang, Jisoo Kim, and Se Young Chun. Multi-temporal recurrent neural networks for progressive non-uniform single image deblurring with incremental temporal training. In *European Conference on Computer Vision*, pages 327–343. Springer, 2020. 2
- [28] Adam Paszke, Sam Gross, Soumith Chintala, Gregory Chanan, Edward Yang, Zachary DeVito, Zeming Lin, Alban Desmaison, Luca Antiga, and Adam Lerer. Automatic differentiation in pytorch. 2017. 6
- [29] Henri Rebecq, Daniel Gehrig, and Davide Scaramuzza. Esim: an open event camera simulator. In *Conference on Robot Learning*, pages 969–982. PMLR, 2018. 6
- [30] Henri Rebecq, René Ranftl, Vladlen Koltun, and Davide Scaramuzza. High speed and high dynamic range video with an event camera. *IEEE transactions on pattern analysis and machine intelligence*, 2019. 1
- [31] Wei Shang, Dongwei Ren, Dongqing Zou, Jimmy S. Ren, Ping Luo, and Wangmeng Zuo. Bringing events into video deblurring with non-consecutively blurry frames. In *Proceedings of the IEEE/CVF International Conference on Computer Vision (ICCV)*, pages 4531–4540, October 2021. 2
- [32] Wang Shen, Wenbo Bao, Guangtao Zhai, Li Chen, Xiongkuo Min, and Zhiyong Gao. Blurry video frame interpolation. In *Proceedings of the IEEE/CVF Conference on Computer Vision and Pattern Recognition*, pages 5114–5123, 2020. 1
- [33] Shuochen Su, Mauricio Delbracio, Jue Wang, Guillermo Sapiro, Wolfgang Heidrich, and Oliver Wang. Deep video deblurring for hand-held cameras. In *Proceedings of the IEEE Conference on Computer Vision and Pattern Recognition*, pages 1279–1288, 2017. 2, 6
- [34] Peng Sun, Wenhu Zhang, Huanyu Wang, Songyuan Li, and Xi Li. Deep rgb-d saliency detection with depth-sensitive attention and automatic multi-modal fusion. In *Proceedings of the IEEE/CVF Conference on Computer Vision and Pattern Recognition*, pages 1407–1417, 2021. 5
- [35] Xin Tao, Hongyun Gao, Xiaoyong Shen, Jue Wang, and Jiaya Jia. Scale-recurrent network for deep image deblurring. In *Proceedings of the IEEE Conference on Computer Vision and Pattern Recognition*, pages 8174–8182, 2018. 2
- [36] Fu-Jen Tsai, Yan-Tsung Peng, Yen-Yu Lin, Chung-Chi Tsai, and Chia-Wen Lin. Banet: Blur-aware attention networks for dynamic scene deblurring. *arXiv preprint arXiv:2101.07518*, 2021. 6, 7
- [37] Stepan Tulyakov, Daniel Gehrig, Stamatios Georgoulis, Julius Erbach, Mathias Gehrig, Yuanyou Li, and Davide Scaramuzza. TimeLens: Event-based video frame interpolation. *IEEE Conference on Computer Vision and Pattern Recognition*, 2021. 6
- [38] Ashish Vaswani, Noam Shazeer, Niki Parmar, Jakob Uszkoreit, Llion Jones, Aidan N Gomez, Łukasz Kaiser, and Illia Polosukhin. Attention is all you need. In *NIPS*, pages 5998–6008, 2017. 2
- [39] Bishan Wang, Jingwei He, Lei Yu, Gui-Song Xia, and Wen Yang. Event enhanced high-quality image recovery. In *European Conference on Computer Vision*. Springer, 2020. 1
- [40] Lin Wang, Yujeong Chae, and Kuk-Jin Yoon. Dual transfer learning for event-based end-task prediction via pluggable event to image translation. In *ICCV*, 2021. 1
- [41] Lin Wang, Yujeong Chae, Sung-Hoon Yoon, Tae-Kyun Kim, and Kuk-Jin Yoon. Evidistill: Asynchronous events to end-task learning via bidirectional reconstruction-guided cross-modal knowledge distillation. In *Proceedings of the IEEE/CVF Conference on Computer Vision and Pattern Recognition*, pages 608–619, 2021. 1
- [42] Lin Wang, Tae-Kyun Kim, and Kuk-Jin Yoon. Eventsr: From asynchronous events to image reconstruction, restoration, and super-resolution via end-to-end adversarial learning. In *CVPR*, pages 8315–8325, 2020. 1
- [43] Xintao Wang, Kelvin C.K. Chan, Ke Yu, Chao Dong, and Chen Change Loy. Edvr: Video restoration with enhanced deformable convolutional networks. In *Proceedings of the IEEE/CVF Conference on Computer Vision and Pattern Recognition (CVPR) Workshops*, June 2019. 2
- [44] Zhou Wang, Alan C Bovik, Hamid R Sheikh, and Eero P Simoncelli. Image quality assessment: from error visibility to structural similarity. *IEEE transactions on image processing*, 13(4):600–612, 2004. 6
- [45] Patrick Wieschollek, Michael Hirsch, Bernhard Scholkopf, and Hendrik Lensch. Learning blind motion deblurring. In *ICCV*, pages 231–240, 2017. 1, 2
- [46] Sanghyun Woo, Jongchan Park, Joon-Young Lee, and In So Kweon. Cbam: Convolutional block attention module. In *Proceedings of the European Conference on Computer Vision (ECCV)*, September 2018. 6
- [47] Yuxin Wu and Kaiming He. Group normalization. In *Proceedings of the European conference on computer vision (ECCV)*, pages 3–19, 2018. 5
- [48] Fang Xu, Lei Yu, Bishan Wang, Wen Yang, Gui-Song Xia, Xu Jia, Zhendong Qiao, and Jianzhuang Liu. Motion deblurring with real events. In *Proceedings of the IEEE/CVF International Conference on Computer Vision (ICCV)*, pages 2583–2592, October 2021. 2
- [49] Syed Waqas Zamir, Aditya Arora, Salman Khan, Munawar Hayat, Fahad Shahbaz Khan, Ming-Hsuan Yang, and Ling Shao. Multi-stage progressive image restoration. *arXiv preprint arXiv:2102.02808*, 2021. 2, 6, 7, 8
- [50] Hongguang Zhang, Yuchao Dai, Hongdong Li, and Piotr Koniusz. Deep stacked hierarchical multi-patch network for image deblurring. In *Proceedings of the IEEE/CVF Conference on Computer Vision and Pattern Recognition*, pages 5978–5986, 2019. 1, 2, 6, 7, 8
- [51] Kaihao Zhang, Wenhan Luo, Yiran Zhong, Lin Ma, Wei Liu, and Hongdong Li. Adversarial spatio-temporal learning for video deblurring. *IEEE Transactions on Image Processing*, 2018. 2
- [52] Kaihao Zhang, Wenhan Luo, Yiran Zhong, Lin Ma, Bjorn Stenger, Wei Liu, and Hongdong Li. Deblurring by realistic blurring. In *Proceedings of the IEEE/CVF Conference on Computer Vision and Pattern Recognition*, pages 2737–2746, 2020. 2, 6, 7
- [53] Kaihao Zhang, Wenhan Luo, Yiran Zhong, Lin Ma, Bjorn Stenger, Wei Liu, and Hongdong Li. Deblurring by realistic blurring. In *Proceedings of the IEEE/CVF Conference*

on *Computer Vision and Pattern Recognition (CVPR)*, June 2020. [2](#)

- [54] Limeng Zhang, Hongguang Zhang, Chenyang Zhu, Shasha Guo, Jihua Chen, and Lei Wang. Fine-grained video deblurring with event camera. In *ICMM*, pages 352–364. Springer, 2021. [1](#)
- [55] Miao Zhang, Sun Xiao Fei, Jie Liu, Shuang Xu, Yongri Piao, and Huchuan Lu. Asymmetric two-stream architecture for accurate rgb-d saliency detection. In *European Conference on Computer Vision*, pages 374–390. Springer, 2020. [5](#)
- [56] Youjian Zhang, Chaoyue Wang, and Dacheng Tao. Video frame interpolation without temporal priors. *Advances in Neural Information Processing Systems*, 33, 2020. [1](#), [6](#)
- [57] Zhihang Zhong, Ye Gao, Yinqiang Zheng, and Bo Zheng. Efficient spatio-temporal recurrent neural network for video deblurring. In *European Conference on Computer Vision*, pages 191–207. Springer, 2020. [2](#), [4](#), [6](#), [7](#), [8](#)
- [58] Shangchen Zhou, Jiawei Zhang, Jinshan Pan, Haozhe Xie, Wangmeng Zuo, and Jimmy Ren. Spatio-temporal filter adaptive network for video deblurring. In *Proceedings of the IEEE/CVF International Conference on Computer Vision (ICCV)*, October 2019. [2](#), [6](#)
- [59] Alex Zihao Zhu, Liangzhe Yuan, Kenneth Chaney, and Kostas Daniilidis. Unsupervised event-based learning of optical flow, depth, and egomotion. In *Proceedings of the IEEE/CVF Conference on Computer Vision and Pattern Recognition*, pages 989–997, 2019. [4](#), [6](#)
- [60] Yunhao Zou, Yinqiang Zheng, Tsuyoshi Takatani, and Ying Fu. Learning to reconstruct high speed and high dynamic range videos from events. In *Proceedings of the IEEE/CVF Conference on Computer Vision and Pattern Recognition*, pages 2024–2033, 2021. [1](#)